Topological Properties of the Structural Brain Network in Autism via ε-Neighbor Method

Min-Hee Lee, Dong Youn Kim, Moo K. Chung, Andrew L. Alexander, and Richard J. Davidson

Abstract*—*Objective: **Topological characteristics of the brain can be analyzed using structural brain networks constructed by diffusion tensor imaging (DTI). When a brain network is constructed by the existing parcellation method, the structure of the network changes depending on the scale of parcellation and arbitrary thresholding. To overcome these issues, we propose to construct brain networks using the improved ε-neighbor construction, which is a parcellation free network construction technique. *Methods:* We acquired DTI from 14 control subjects and 15 subjects with autism. We examined the differences in topological properties of the brain networks constructed using the proposed method and the existing parcellation between the two groups. *Results:* As the number of nodes increased, the connectedness of the network decreased in the parcellation method. However, for brain networks constructed using the proposed method, connectedness remained at a high level even with an increase in the number of nodes. We found significant differences in several topological properties of brain networks constructed using the proposed method, whereas topological properties were not significantly different for the parcellation method. *Conclusion:* The brain networks constructed using the proposed method are considered as more realistic than a parcellation method with respect to the stability of connectedness. We found that subjects with autism showed the abnormal characteristics in the brain networks. These results demonstrate that the proposed method may provide new insights to analysis in the structural brain network. *Significance:* We proposed the novel brain network construction method to overcome the shortcoming in the existing parcellation method.**

***Index Terms*—Autism, diffusion tensor imaging (DTI), ε-neighbor construction method, parcellation, structural brain network, topological properties.**

I. Introduction

THE human brain is a complex system capable of generating and integrating information from multiple sources in a highly efficient manner [1]. Defining the global architecture of the anatomical connection patterns of the human brain is important, because these connection patterns can provide new insights into correlations between functional brain disorders and underlying structural collapses [2], [3]. Diffusion tensor imaging (DTI) is a technique that facilitates non-invasive studies of the living human brain. Using DTI data, white matter tractography can determine the fiber bundle direction at each pixel and allow visualization of fiber bundles. The development of this technique has yielded large datasets of anatomical connection patterns [4]. Sporns *et al*. inferred the human brain connectome by using the DTI data, thus comprehensively describing the structure of element networks and connections forming the human brain [3]. Recently, attempts to model the human brain as a network of brain regions connected by anatomical tracts or functional associations have attracted considerable interest, because characterizing this structural and functional connectivity could impact studies of brain pathology and developmental disorders [5]. Comparisons of structural or functional network topological properties between subjects could reveal putative connectivity abnormalities in neurological and psychiatric disorders [4].

A network is set of nodes linked by edges. Nodes in a neural network correspond to individual neurons at the microscopic scale, but it is unclear how grey matter should be parcellated at the macroscopic scale [6]. In many studies, nodes are composed using the parcellation method [2], [6], [7], which is somewhat problematic in that the network structure is influenced by changes in both the parcellation scale and thresholding in connectivity matrices. Various topological parameters depend on the choice of threshold. Because the topological properties of nodes changes according to parcellation scale, Zalesky *et al*. investigated how topological properties of the network, such as normalized path length, average normalized clustering coefficient, small-worldness, and node degree changed according to the parcellation scale used to divide brain regions. They argued that the parcellation scale should be carefully determined in structural brain network analysis [6].

To overcome these problems, Chung *et al*. proposed a network graph modeling technique called the ε-neighbor construction that does not use parcellation schemes [8]. The ε-neighbor method iteratively considers only two endpoints of each tract, designated as nodes on the graph, whereas tracts are designated as edges [8]. In this study, we improved the ε-neighbor construction method and evaluated the topological properties of structural brain networks obtained from the existing parcellation method and the ε-neighbor construction.

Manuscript received September 21, 2017; revised November 24, 2017; accepted January 3, 2018. Date of publication January 15, 2018; date of current version September 18, 2018. This work was supported by the Brain Research Program through the National Research Foundation of Korea funded by the Ministry of Science, ICT, and Future Planning (2016M3C7A1905385) and NIH Brain Initiative Grant R01 EB022856. *(Corresponding author: Moo K. Chung.)*

M. H. Lee and D. Y. Kim are with the Department of Biomedical Engineering, Yonsei University.

M. K. Chung is with the Waisman Laboratory for Brain Imaging and Behavior, University of Wisconsin, Madison, WI 53706 USA (e-mail: mkchung@wisc.edu).

A. L. Alexander and R. J. Davidson are with the Waisman Laboratory for Brain Imaging and Behavior, University of Wisconsin.

Digital Object Identifier 10.1109/TBME.2018.2794259

Many neuropsychiatric disorders are considered to reflect abnormalities in brain connectivity [9]. Autism is a neurodevelopmental disorder characterized by impaired communication, social interaction, and social comprehension [10]. The increasing prevalence of autism has promoted interest in understanding brain functional and structural connectivity in this neurodevelopmental disorder [11]. Many studies have used functional magnetic resonance imaging (fMRI) to analyze and characterize functional connectivity in autism [12]–[15]. Cherkassky *et al*. observed lower functional connectivity in the left hemisphere in autism [13]. Belmonte *et al*. observed local functional over-connectivity and global functional under-connectivity in autism [12]. However, some studies reported that global under-connectivity was not always observed in autism, and concluded that observations of abnormal over-connectivity and under-connectivity require further investigation [14], [15].

Other studies have used DTI in studying autism [8], [9], [16], [17]. Chung *et al*. reported that the brain networks in autism exhibited slower integration rates and have more nodes with a low degree of connectivity, thus demonstrating over-connectivity [8], [17] Using the edge weight distribution, Adluru *et al*. reported differences in autism [16]. Dennis *et al*. reported that carriers of a common variant in the autism risk gene, CNTNAP2, had differences in structural connectivity. They found that subjects with autism had a shorter characteristic path length, greater small-worldness, and greater global efficiency in the left hemisphere, and greater global efficiency in the right hemisphere [9]. Rudie *et al*. examined differences in topological properties in both structural and functional connectivities in autism. They reported differences in topological properties of functional connectivity [18]. However, they did not observe differences in the topological properties of structural connectivity.

To determine if there are differences in structural connectivity in autism, we applied the improved ε-neighbor construction method to analyze and compare topological properties between brain networks derived from 14 control subjects and 15 subjects with autism.

II. Network Construction Methods

A. ε-Neighbor Construction Method

In this section, we explain the ε-neighbor construction method in detail. Suppose the entire brain contains n tracts. The i-th tract will have two endpoints, e_{i1} and e_{i2}. In the network graph construction, we only consider the two endpoints at a time. The endpoints of tract are considered to be nodes; tracts are considered to be edges in the graph.

Let $G_k = \{V_k, E_k\}$ be a 3D graph with node set V_k and edge set E_k at the k-th iteration. The distance between point p to the graph G_k to be the shortest Euclidean distance between p and all points in V_k:

$$d(p, G_k) = \min_{q \in V_k} ||p - q|| \tag{1}$$

Point p is designated an ε-neighbor of graph G_k if $d(p, G_k) \leq \varepsilon$. Because ε is related to the scale at which the graph is constructed, ε is considered to be a measure of graph resolution. If ε has a large value, the constructed graph will have fewer nodes. If ε has a small value, the constructed graph will have more nodes. The ε-neighbor construction method is performed in order from the longest tract to the shortest tract.

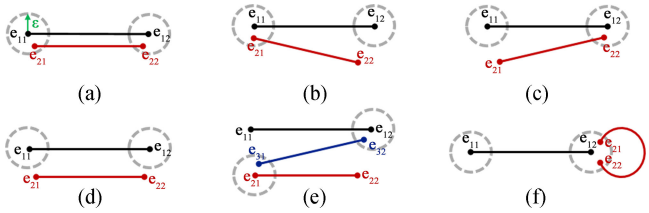

Fig. 1. Six possibilities of the ε-neighbor construction: (a) e_{21} and e_{22} are all ε-neighbors of G_1. (b) Only e_{21} is an ε-neighbor of G_1. (c) Only e_{22} is an ε-neighbor of G_1. (d) Neither e_{21} nor e_{22} is an ε-neighbor of G_1. (e) e_{31} is an ε-neighbor of e_{21} in G_2 and e_{32} is an ε-neighbor of e_{12} in G_2. (f) e_{21} and e_{22} are ε-neighbors of e_{11} or e_{12} in G_1. This case is considered to be noise, because it resulted in a circular tract.

Starting with two endpoints e_{11} and e_{12} of the first tract which has the longest length of tracts, the ε-neighbor construction method begins with graph G_1, with $V_1 = \{e_{11}, e_{12}\}$ and $E_1 = \{e_{11}e_{12}\}$. Next, the endpoints e_{21} and e_{22} from the second longest tract are added to the existing graph G_1. Fig. 1 shows six possibilities of adding the second tract to graph G_1.

In Fig. 1(a), e_{21} and e_{22} are all ε-neighbors of G_1. Because the endpoints e_{21} and e_{22} are close to the existing graph G_1, node set V_1 and edge set E_1 do not change. Thus, $V_2 = V_1$ and $E_2 = E_1$.

In Fig. 1(b), only e_{21} is an ε-neighbor of G_1. Node e_{22} is added to node set V_1, and edge $e_{21}e_{22}$ is added to edge set E_1. Thus, $V_2 = V_1 \cup \{e_{22}\}$ and $E_2 = E_1 \cup \{e_{21}e_{22}\}$.

In Fig. 1(c), only e_{22} is an ε-neighbor of G_1. Node e_{21} is added to node set V_1, and edge $e_{21}e_{22}$ is added to edge set E_1. Thus, $V_2 = V_1 \cup \{e_{21}\}$ and $E_2 = E_1 \cup \{e_{21}e_{22}\}$.

In Fig. 1(d), neither e_{21} nor e_{22} is an ε-neighbor of G_1. Nodes e_{21}, e_{22} are added to node set V_1, and edge $e_{21}e_{22}$ is added to edge set E_1. Thus, $V_2 = V_1 \cup \{e_{21}, e_{22}\}$ and $E_2 = E_1 \cup \{e_{21}e_{22}\}$.

In Fig. 1(e), e_{31} is an ε-neighbor of e_{21} in G_2 and e_{32} is an ε-neighbor of e_{12} in G_2. The node set V_3 does not change; however, edge $e_{31}e_{32}$ is added to edge set E_2. Thus, $V_3 = V_2$ and $E_3 = E_2 \cup \{e_{31}e_{32}\}$.

In Fig. 1(f), e_{21} and e_{22} are ε-neighbors of either e_{11} or e_{12} in G_1. This relationship is considered to be noise since they result in a circular tract. Thus, $V_2 = V_1$ and $E_2 = E_1$. Previously in Chung *et al*., this case was simply ignored thus resulting in an additional noise in the network construction [8].

Fig. 2 shows a toy example for the ε-neighbor construction process. Fig. 2(a) represents five sample tracts. The ε-neighbor construction starts from graph G_1, which has $V_1 = \{e_{11}, e_{12}\}$ and $E_1 = \{e_{11}e_{12}\}$ as in Fig. 2(b). Next, the endpoints of the second longest tract (e_{21}, e_{22}) are used. Neither e_{21} nor e_{22} is an ε-neighbor of G_1. Thus, $V_2 = V_1 \cup \{e_{21}, e_{22}\}$ and $E_2 = E_1 \cup \{e_{21}e_{22}\}$ as in Fig. 2(c). In step 3, we use endpoints of the third longest tract (e_{31}, e_{32}). e_{32} is an ε-neighbor of G_2. Thus,

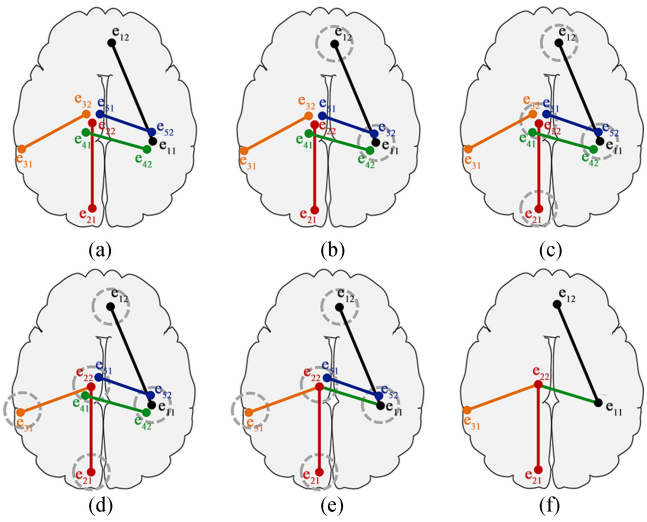

Fig. 2. Toy example of the network construction process using the ε-neighbor construction method. (a) Five sample tracts. (b) The ε-neighbor construction starts from graph G_1, which has $V_1 = \{e_{11}, e_{12}\}$ and $E_1 = \{e_{11}e_{12}\}$. (c) Neither e_{21} nor e_{22} is an ε-neighbor of G_1. Thus, $V_2 = V_1 \cup \{e_{21}, e_{22}\}$ and $E_2 = E_1 \cup \{e_{21}e_{22}\}$. (d) e_{32} is an ε-neighbor of G_2. Thus, $V_3 = V_2 \cup \{e_{31}\}$ and $E_3 = E_2 \cup \{e_{31}e_{32}\}$. (e) e_{41} is an ε-neighbor of e_{22} in G_3 and e_{42} is an ε-neighbor of e_{11} in G_3. Thus, $V_4 = V_3$ and $E_4 = E_3 \cup \{e_{41}e_{42}\}$. (f) e_{51} and e_{52} are all ε-neighbors of G_4. Thus, $V_5 = V_4$ and $E_5 = E_4$.

$V_3 = V_2 \cup \{e_{31}\}$ and $E_3 = E_2 \cup \{e_{31}e_{32}\}$ as in Fig. 2(d). In step 4, we use the endpoints of the fourth longest tract (e_{41}, e_{42}). e_{41} is an ε-neighbor of e_{22} in G_3 and e_{42} is an ε-neighbor of e_{11} in G_3. Thus, $V_4 = V_3$ and $E_4 = E_3 \cup \{e_{41}e_{42}\}$ as in Fig. 2(e). Finally, we use the endpoints of the last longest tract (e_{51}, e_{52}). e_{51} and e_{52} are all ε-neighbors of G_4. Thus, $V_5 = V_4$ and $E_5 = E_4$ as in Fig. 2(f).

Fig. 3 shows the brain network constructed using the ε-neighbor construction and the existing parcellation method. The resulting 3D graphs are represented using adjacency matrices. The adjacency matrix $A = (adj_{ij})$ is defined as follows. If nodes i and j are connected, $adj_{ij} = 1$, otherwise $adj_{ij} = 0$.

B. Parcellation Method

We also constructed the brain network using the parcellation method for the comparison. We used the automated anatomical labeling (AAL) template, which parcellates the brain into 116 regions [19]. Let $P(i)$ denote the i-th parcellation. The weighted adjacency matrix $W = (w_{ij})$ for the AAL parcellation was defined as

$$w_{ij} = \sum_{k=1}^{n} I_{\{e_{k1} \in P(i)\}} I_{\{e_{k2} \in P(j)\}} + I_{\{e_{k1} \in P(j)\}} I_{\{e_{k1} \in P(i)\}}, \tag{2}$$

where the indicator function $I_{\{e_{k1} \in P(i)\}} = 1$ if $e_{k1} \in P(i)$ and 0 otherwise [6]. Since some topological properties of weighted graphs are ill-defined [6], we only considered binary graphs. We binarized weighted adjacency matrix further by assigning one to all non-zero entries for each weighted adjacency matrix. (Fig. 3(b)).

III. Complex Network Analysis

Complex networks have received recent attention from a range of disciplines, including social science, information science, biology, and physics [1]. Numerous studies have analyzed networks according to their topological properties [2], [6], [20], [21]. Complex network analysis is an approach that characterizes datasets and describes the properties of complex systems by quantifying the topologies of the associated networks. Complex network analysis is based on graph theory, a mathematical approach for studying networks [4]. In this study, we used the following topological properties: path length, global efficiency (E_{glob}), clustering coefficient, local efficiency (E_{loc}) node degree, density, node betweenness centrality (NBC), and regional efficiency (E_{reg}).

A. Path Length

Functional integration in the brain is the ability to combine information from multiple brain regions. A measure of this integration is often based on the concept of path length. Path length measures the ability to integrate information flow and functional proximity between pairs of brain regions [1], [4]. When the path length becomes shorter, the potential for functional integration increases [1]. The path length equal to the number of edges in the path [1].

B. Clustering Coefficient

Clustering coefficient describes the ability for functional segregation and efficiency of local information transfer. Clustering coefficient at a node is calculated as the number of existing connections between the neighbors of the node divided by the number of all possible connections [22]. The clustering coefficient C for the graph is then calculated as the average clustering coefficient over all the nodes.

C. Small-World

The small-world method of network analysis, with clustering coefficient C and average path length L, was proposed by Watts and Strogatz [22]. A real network was considered to be a small-world network if it met the following criteria:

$$\begin{aligned} \gamma &= C^{\text{real}}/C^{\text{rand}} \gg 1 \\ \lambda &= L^{\text{real}}/L^{\text{rand}} \approx 1 \\ \sigma &= \gamma/\lambda > 1 \end{aligned} \tag{3}$$

where C^{real} and L^{real} are the average clustering coefficient and characteristic path length of real network. C^{rand} and L^{rand} are the average clustering coefficient and characteristic path length of random networks that preserved the number of nodes, edges, and node degree distributions present in the real network. In our experiment, we used 100 random networks for each real network. Recent studies have demonstrated that human brain networks derived from DTI have small-world properties [2], [6], [23]. Small-world networks have high clustering coefficients and short path lengths and might provide the underlying

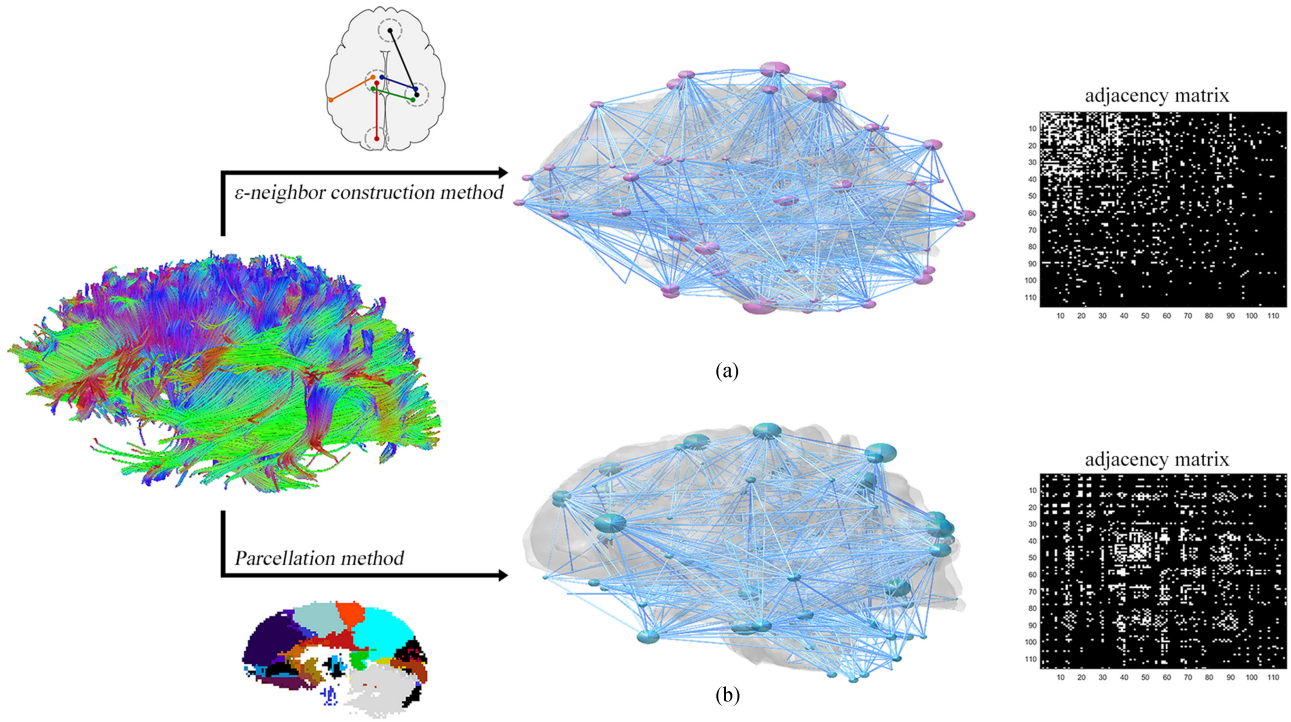

Fig. 3. (a) Structural brain network constructed by the ε-neighbor construction. Nodes are located in the center of ε sphere. (b) Structural brain network constructed by the AAL parcellation method. Nodes are located in the mass center of each AAL region.

structural substrates of functional integration and segregation in the human brain [2].

D. Network Efficiency

Regional efficiency E_{reg} measures the average path length between a given node and the remaining nodes [7] and reflects the integration of each node [25]. Given node i, it is defined as

$$E_{\mathrm{reg}}(i) = \frac{1}{n-1}\sum_{i\neq j}\frac{1}{d_{ij}}, \tag{4}$$

where d_{ij} is the shortest path length between nodes i and j and n is the total number of nodes.

Local efficiency E_{loc} measures the fault-tolerance of the network and ability of information exchange in sub-networks [26]. It measures the efficiency of the connections between the nearest neighborhoods of a node [24].

Global efficiency E_{glob} is defined as the average of the inverse of the shortest path length between nodes [24]. The E_{glob} of a brain network refers to the efficiency of parallel information transfer in the network [24] and reflects integration over the whole brain network [25].

E. Node Degree

Node degree in a graph is defined as the numbers of connections with other nodes. Typically, node degree is calculated as the average for all the nodes. A node with a high degree is interacting with many other nodes in the network [4].

Node degree distribution shows resilience to a targeted attack, i.e., node removal [27], [28]. The human brain network has been considered to be a scale-free network, implying the existence of a few highly connected nodes with superior resilience to random node failures [1], [29]. Recently, studies have claimed that the human brain network is not scale-free [2], [6], [20]. To test for scale-freeness, we fitted the node degree distribution to three degree distributions:

$$\begin{aligned}&\text{power law}: x^{(\alpha-1)}\\ &\text{exponential}: e^{(-x/x_c)}\\ &\text{exponentially truncated power law}: x^{(\alpha-1)}e^{(-x/x_c)},\end{aligned} \tag{5}$$

where x is the node degree value, x_c denotes the estimated cutoff degree, and α is the estimated exponent. The node degree distribution was fitted using the curve fitting toolbox in MATLAB and goodness of fit was assessed by the R-squared values.

F. Density

Network density is measure of the number of connections compared to the maximum possible number of connections between nodes, and indicates how well the network is connected [30]. Biological networks, however, are characterized by a small number of connections [30]. Low densities describe sparse graphs, whereas high densities describe dense graphs [31].

G. Connected Component

A connected component is a sub-graph whose nodes are connected by edges. The number of connected components of the graph is the number of structurally independent or disconnected

sub-graphs. To identify connected components, we used the Dulmage-Mendelsohn decomposition method, a method widely used for decomposing a sparse matrix [32]. The largest connected component was defined as the connected component with the largest number of nodes [33].

Network connectedness refers to how well network nodes are connected. Suppose there is total n number of nodes. If the size of the largest connected component approaches n, the connectedness will increase [34]. In this study, we calculated the size of the largest connected component as a proportion of n.

H. Node Betweenness Centrality

In a complex network, node betweenness centrality (NBC) can be used to determine the relative importance of a node and to represent the communication load. NBC can measure the influence of a node over information flow between other nodes [2]. The betweenness centrality of a given node v is defined as

$$NBC = \sum_{i \neq v \neq j} \frac{\sigma_{ij}(v)}{\sigma_{ij}}, \tag{6}$$

where σ_{ij} is the number of shortest paths between nodes i and j and $\sigma_{ij}(v)$ is the number of shortest paths passing through node v [35], [36].

To understand the connection structure of a network, the node attack was performed [27], [28]. To observe the effects of removing nodes on the network, we calculated the size of largest connected component after removal of a node. Node attacks were performed as follows. 1) For random node attack, we removed randomly chosen nodes until the size of largest connected component becomes zero and repeated this procedure 1000 times. 2) For the targeted node attack, we employed NBC that was used in previous targeted node attack studies [27], [28]. We removed the nodes in decreasing order of their NBC. The removal process continues until the size of largest connected component becomes zero.

We compared the size of largest connected component between two groups for each removal step.

I. Statistical Analysis

Matlab version R2014a (Mathworks, Natick, MA, USA) was used for statistical analysis. In this study, we used a nonparametric permutation t-test for the statistical analysis in all network properties between two groups [37]. We randomly permuted the group labels, and then recomputed two-sample t-statistics between the permuted groups. The permutation was repeated 10000 times. We determined the 95 percentile points of the t-distribution as a critical value (p-value $= 0.05$). The p-values were adjusted for multiple comparisons using the false discovery rate (FDR) correction.

IV. Application

A. Image Acquisition and Processing

We analyzed 29 DTI consisting of 14 normal controls (12.1 ± 2.7 years old, range 10–19) and 15 subjects with autism (13.9 ± 3.3 years old, range 10–22) who were matched for age, handedness, IQ, and head size.

To acquire DTI with more directions, scans take more time and children with autism may have difficulty staying still [38]. Yendiki *et al*. reported that children with autism showed more head motion than typically developing children [39]. The longer scan time causes more head motion [39]. Thus, DTI were obtained for a single ($b = 0$) reference image and 12 non-collinear diffusion-encoding directions, with a diffusion weighting factor of $b = 1000$ s/mm^2.

Distortion associated with eddy currents and head motion for each dataset was adjusted using automated image registration (AIR) [40]. Distortions from field inhomogeneities were adjusted using custom software algorithms [41]. The six tensor elements were calculated using the non-linear fitting methods [42]. We used nonlinear tensor image registration algorithms for spatial normalization of DTI data [43], and performed streamline-based tractography using the TENsor Deflection (TEND) algorithm [44], [45].

B. Comparisons Against Parcellation Method

To compare the ε-neighbor construction method to the existing conventional parcellation method, it was necessary to perform the template normalization. We performed 3D non-linear image registration between fractional anisotropy and AAL templates using Ezys [46]. This enabled us to use both methods in the same normalized space.

To align tracts to AAL parcellation, tract culling was necessary. A tract was considered usable if each endpoint of the tract intersected one of the parcellations in the AAL template. Unusable tracts were culled from the set of all tracts. Moreover, tracts that were less than 10 mm in length were also culled because they were considered to be noise tracts. Culling is a necessary step to eliminate spurious tracts that do not interconnect in the parcellation method [6]. We found that there are many unusable tracts in one subject, which is considered as an outlier. For this reason, one outlying subject was removed in the analysis. After culling tracts, we used the same usable tracts in both methods. The DTI had 3056.7 ± 266.21 culled tracts and 6943.30 ± 266.21 usable tracts (Fig. 4). Approximately 30% of tracts were unusable in the parcellation method.

Since location and the number of nodes in the networks constructed using the ε-neighbor method may be different from networks constructed using the parcellation method, we transformed the ε-neighbor networks to the AAL parcellation. We combined the nodes located in each AAL parcellation into one node.

For pair comparisons, it was also necessary to use the network scales where the basic topological properties of the networks are compatible between the methods. We adjusted the ε-radius in the ε-neighbor construction method and parcellated additional subregions within AAL using the algorithm proposed by Zalesky [6]. This results in networks with 116, 221, 330, 456, and 561 nodes (Fig. 5). We computed the connectedness of the network as a function of the parcellation scale and ε-radius (Table I). The connectedness was close to one for the ε-neighbor

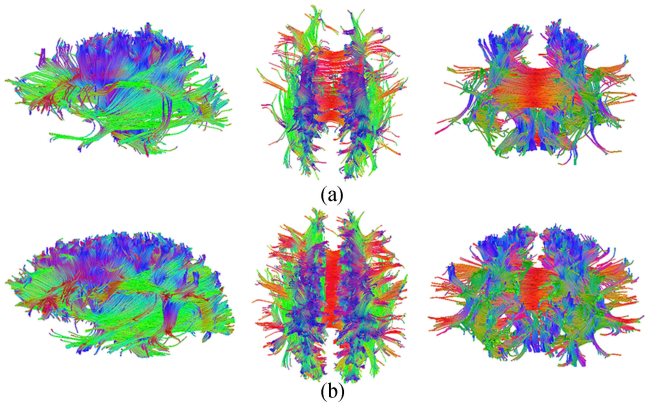

Fig. 4. The results of culling tracts. A tract was considered usable if it intersected one of the parcellations in the AAL template. Tracts with length less than 10 mm were also culled as these were considered to be noisy tracts. Tracts that do not connect any two AAL parcellations are also culled. (a) Culled tracts. (b) Usable tracts.

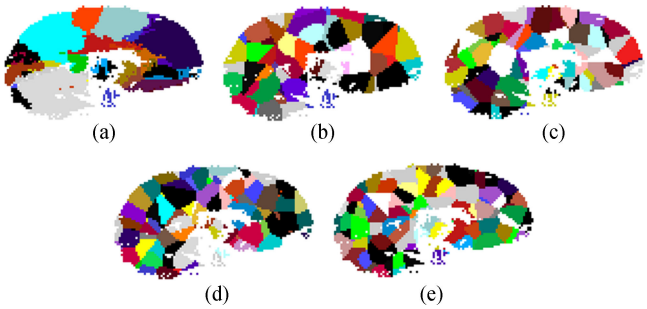

Fig. 5. Results of additional parcellation. To observe how topological properties of the network changed according to the number of nodes, we parcellated additional subregions within AAL parcellations. (a) 116 nodes (b) 221 nodes (c) 330 nodes (d) 456 nodes (e) 561 nodes.

TABLE I
CONNECTEDNESS COMPARISON BETWEEN THE PARCELLATION AND ε-NEIGHBOR CONSTRUCTION METHODS

	Parcellation Method		ε-neighbor Construction	
	Mean	SD	Mean	SD
116 Nodes	0.906	0.025	0.999	0.006
221 Nodes	0.935	0.024	0.999	0.003
330 Nodes	0.887	0.032	0.997	0.004
456 Nodes	0.820	0.033	0.994	0.005
561 Nodes	0.786	0.032	0.993	0.005

SD: standard deviation.

construction regardless of the number of nodes used. On the other hand, connectedness decreased for the parcellation method as the node size increased. Thus, the comparisons were done using 116 and 221 node networks, which results in less than 10% disconnectedness for the parcellation method.

For the ε-neighbor construction method with 116 nodes, significantly higher E_{glob} (t-stat. $= -1.70$, p-value $= 0.05$) and node degree (t-stat. $= -1.96$, p-value $= 0.03$) were observed in autism. For the ε-neighbor construction method with 221 nodes, significantly higher E_{glob} (t-stat. $= -2.81$, p-value $= 0.0053$) and density (t-stat. $= -2.52$, p-value $= 0.0097$) were observed in (Table II). For the parcellation method, we could not observe the differences in topological properties between the two groups.

C. Abnormal Topological Properties in Autism

Since the parcellation method was not sensitive compared to the ε-neighbor construction method, we used the ε-neighbor construction method in characterizing the topological properties of the autistic brain network.

1) Global Properties: To avoid the biased results owing to selection of a specific ε-radius, we had chosen a range of the graph resolution ε-radius (7$\sim$12 mm) with the following conditions. a) The number of nodes is more than 90 (when ε-radius becomes 12 mm) which is frequently used as network scale in previous brain network studies [7], [25], [48] and fewer than 500 (when ε-radius becomes 7 mm) which is often the highest number of nodes used in brain network analysis. b) The number of nodes and edges between two groups are similar to each other.

For comparison of global properties between the two groups, we used the area under curve (AUC). Since all subjects met the small-worldness criteria for a range of ε-radius, the constructed brain networks can be considered to be small-world networks (Fig. 6). Moreover, we could not observe significant differences in small-worldness between the two groups. Small-world networks can be classified into three categories - power law, exponential, and exponentially truncated power law - according to their degree distributions [47]. We found that the node degree distribution fit the best to the exponentially truncated power law (Fig. 7). The exponentially truncated power law model yielded the best fit for the brain network in the normal controls. The estimated parameters were $\alpha = 0.9148$, $x_c = 13.96$ with the R-squared value $R_{ep} = 0.997$ for the normal controls and $\alpha = 0.925$, $x_c = 14$ and the R-squared value $R_{ep} = 0.997$ for autism. The better fit of the data to the exponentially truncated power law indicated that the brain networks had hub nodes and bridge edges [2]. The results are in agreement with previous studies [2], [6].

We compared global topological properties of the brain networks between the groups. The subjects with autism exhibited a significantly shorter average path length (t-stat. $= 2.58$, p-value $= 0.0075$), higher global efficiency (t-stat. $= -2.23$, p-value $= 0.017$), and higher degree (t-stat. $= -2.46$, p-value $= 0.012$). However, we could not observe differences in density, clustering coefficient and local efficiency between the groups. Global properties for the brain network of each subject, including means, standard deviations of AUC, and results of group comparisons using non-parametric permutation t-test, are summarized in Table III and Fig. 8.

2) The Effects of Node Attack: Many network measures are influenced by the number of nodes and edges in the network [4]. We choose the graph resolution such that outliers or significant differences in the numbers of nodes and edges between the groups did not exist. We used the ε-radius of 7mm. This resolution is the smallest integer that produced fewer than 500 nodes to reduce computational complexity.

TABLE II
DIFFERENCES IN GLOBAL PROPERTIES BETWEEN CONTROL SUBJECTS AND SUBJECTS WITH AUTISM FOR THE ε-NEIGHBOR CONSTRUCTION METHODS

		Control		Autism		Group Differences		
		Mean	SD	Mean	SD	t-statistics	p-value	Corrected p-value
116 Nodes	Global Efficiency	0.471	0.013	0.478	0.011	−1.692	0.050*	0.072
	Local Efficiency	0.538	0.032	0.546	0.027	−0.754	0.237	0.237
	Density	0.106	0.008	0.110	0.007	−1.678	0.054	0.072
	Degree	12.17	0.605	12.74	0.880	−1.958	0.032*	0.072
221 Nodes	Global Efficiency	0.391	0.006	0.398	0.007	−2.810	0.005**	0.020*
	Local Efficiency	0.362	0.018	0.361	0.031	0.148	0.442	0.442
	Density	0.046	0.002	0.049	0.004	−2.516	0.010**	0.020*
	Degree	10.34	0.203	10.531	0.407	−1.530	0.068	0.091

SD: standard deviation; *: Significant at the 0.05 level; **: Significant at the 0.01 level.

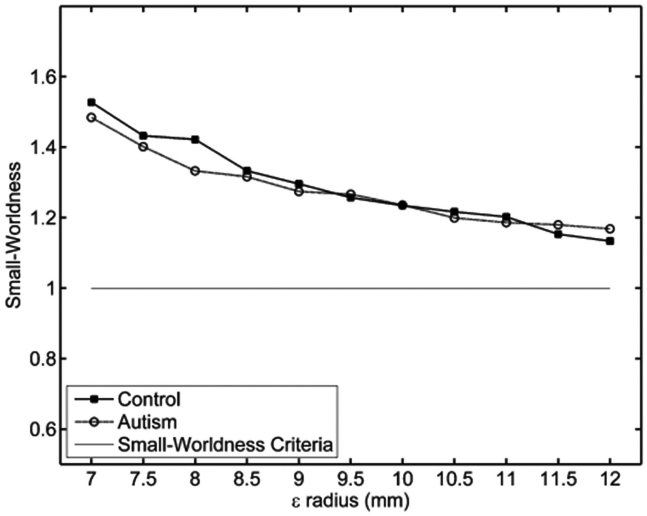

Fig. 6. Assessment of small-worldness as a function of ε radius in the structural brain network of control subjects and subjects with autism. Control subjects and subjects with autism met the small-worldness criteria for all ε radius. There was no significant difference in the area under curve of small-worldness between the two groups.

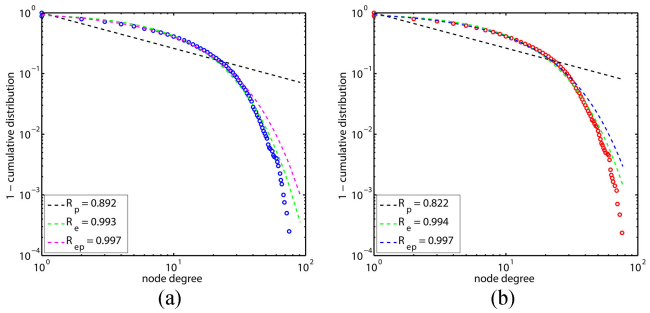

Fig. 7. Degree distribution of the brain network. The power law, exponential and exponentially truncated power law were fitted. R-square was calculated to determine the good of fit. R-squares for the power law (R_p), the exponential (R_e), and exponentially truncated power law (R_{ep}) were computed for autism (a) and normal controls (b). Blue and red circles are the log-log plot of cumulative node degree distribution.

We performed the random and targeted node attacks. We found that the brain networks were more vulnerable to targeted node attack than random node attack and it is consistent with prior studies [27], [48]. We could not detect statistical difference in the size of largest connected component for the random attack. However, we detected statistically significant difference in the size of largest connected component in the targeted node attack over 9 to 33 of removed nodes (p-value < 0.05) (Fig. 9).

3) Regional Efficiency: We also investigated if there were alterations in the regional characteristic of the whole brain networks in autism. We compared regional efficiency E_{reg} for each region and specific resolution (ε-radius of 7mm). Since the locations of nodes are different across subjects, we averaged E_{reg} across the same AAL parcellation. All nodes showed higher regional efficiency in autism. In particular, we observed increased E_{reg} in the right superior temporal gyrus (t-stat. $= -2.40$, p-value $= 0.01$) and left middle temporal gyrus (t-stat. $= -2.30$, p-value $= 0.01$) in autism relative to the normal controls (Fig. 10).

V. VALIDATION

To investigate the sensitivity of the order in which streamlines were used in the ε-neighbor method, we randomly ordered tracts and applied the same procedure. Since the brain network constructed by randomly ordered tracts may produce different results, we generated 1000 brain networks constructed by randomly ordering the tracts. The resulting p-values were then averaged.

Since the number of nodes and edges influences the topological properties [4], it was necessary to compare networks with the similar number of nodes and edges. We found that there is no statistically significant differences in the number of nodes and edges between the brain networks constructed by the sorted tract length for ε-radii 7, 7.5, 8, ... 11, 11.5, 12 mm and randomly ordered tracts for ε-radii 6.8, 7.3, 7.5, ... 11.3, 11.8 mm (p-value > 0.15). Thus, we used these radii for comparisons.

We could not find statistically significant differences in topological properties including density, connectedness path length, clustering coefficient, global efficiency, local efficiency and degree between the brain networks constructed with ordered lengths and random ordered lengths on the same network scales (p-value > 0.3).

The main advantage of using the ordered length of tracts over randomly ordered length is computation. The construction of

TABLE III
GROUP DIFFERENCES IN AREA UNDER CURVE OF GLOBAL PROPERTIES

	Control		Autism		Group Differences		
	Mean	SD	Mean	SD	t-statistics	p-value	Corrected p-value
Path length	12.351	0.165	12.191	0.163	2.582	0.008**	0.040*
Global efficiency	2.301	0.030	2.328	0.034	−2.232	0.017*	0.040*
Clustering coefficient	1.772	0.083	1.809	0.1028	−1.052	0.154	0.180
Local efficiency	2.631	0.090	2.686	0.125	−1.338	0.102	0.143
Small-worldness	6.421	0.274	6.374	0.313	0.405	0.348	0.348
Density	0.482	0.018	0.496	0.025	−1.722	0.049*	0.086
Degree	67.912	1.932	70.410	3.332	−2.465	0.012*	0.040*

SD: standard deviation; *: Significant at the 0.05 level; **: Significant at the 0.01 level.

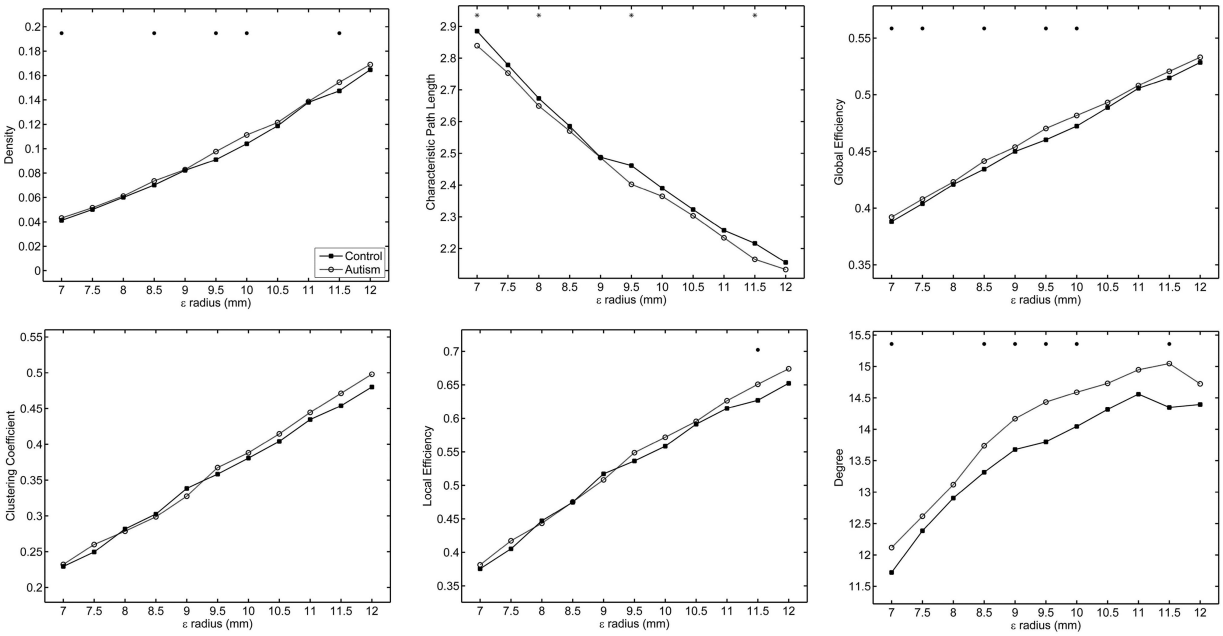

Fig. 8. Comparisons of topological properties between control subjects and subjects with autism. For statistical analysis, area under curve was calculated for each global property. Asterisk (*) means that control subjects have higher value of topological property than subjects with autism at a given ε radius ($p < 0.05$). Dot (.) means that subjects with autism have lower value of topological property than control subjects at a given ε radius ($p < 0.05$). We observed significant differences in area under curve of density, characteristic path length, global efficiency, and degree between two groups.

1000 brain networks using randomly ordered tracts took approximately 90 hours for parallel computation on a quad-core machine. However, construction of brain networks using the sorted tract length took approximately 5 minutes on the same computer. Thus, the use of sorted tract length in determining the order of tracts to use was appropriate.

Since it is difficult to obtain real data with the ground truth, we performed a simulation study. We combined 14 control subjects and 15 subjects with autism and randomly split them evenly so that Group I has 7 normal controls and 7 subjects with autism while Group II has 7 normal controls and 8 subjects with autism. It is expected that there is no group difference between Group I and Group II. This process is repeated 10000 times to ensure that the desired error rate is controlled. We did not detect the difference in topological properties between the randomly split groups (p-values ≥ 0.4). This controlled experiment shows that our method does not produce the false positives in the null data.

VI. DYNAMIC ε-NEIGHBOR CONSTRUCTION

The proposed ε-neighbor static in a sense that the node coordinates are always the coordinates of one of the endpoints of tracts. We also considered a dynamic ε-neighbor method, where we adjusted the center of ε-balls at each iteration. The procedure is identical to the static ε-neighbor construction method except that we also adjust the coordinates of nodes when a new endpoint was merged to the existing graph. It is based illustrated using an example (Fig. 11). (a) The initial graph G_1 consists of node set $V_1 = \{e_{11}, e_{12}\}$ and edge set $E_1 = \{e_{11}e_{12}\}$. (b) e_{21} and e_{22} are ε-neighbors of G_1. New center coordinates are $e'_{11} = (e_{11} + e_{21})/2$ and $e'_{12} = (e_{12} + e_{22})/2$. G_2 consists of $V_2 = \{e'_{11}, e'_{12}\}$ and $E_2 = \{e'_{11}e'_{12}\}$. (c) e_{31} is an ε-neighbor of G_2. The new center coordinates are $e''_{11} = (e_{11} + e_{21} + e_{31})/3$. G_3 consists of $V_3 = \{e''_{11}, e'_{12}, e_{32}\}$ and $E_3 = \{e''_{11}e'_{12}, e''_{11}e_{32}\}$. (d) e_{41} is an ε-neighbor of G_3 and the center coordinates are updated to $e'_{32} = (e_{32} + e_{41})/2$. Thus,

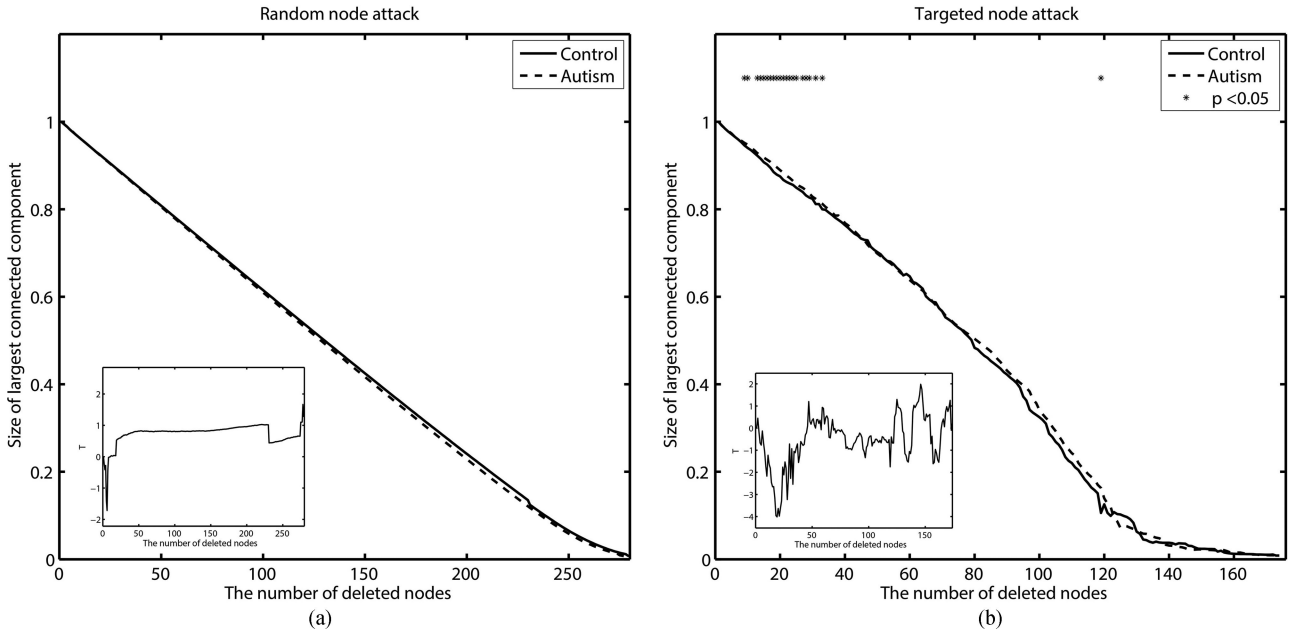

Fig. 9. The change in size of largest connected component over the number of deleted nodes during the random node attack (a) and the targeted node attack (b). In the random node attack, there is no statistically significant difference between the groups. In the targeted node attack, the significant differences are observed. The asterisk indicates that subjects with autism have bigger connected component than the normal controls at the given removal step ($p < 0.05$).

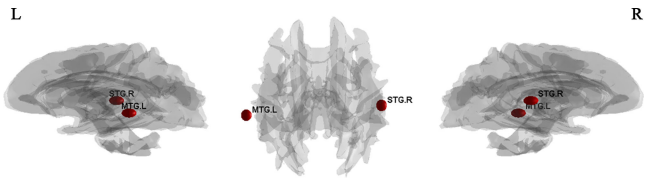

Fig. 10. Disrupted nodes in autism. Higher regional efficiency nodes in autism relative to the normal controls ($p < 0.05$). STG.R, right superior temporal gyrus; MTG.L, left middle temporal gyrus.

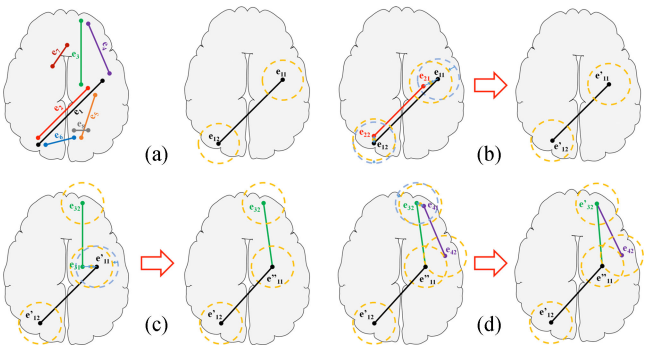

Fig. 11. Toy example of dynamic ε-neighbor construction method.

$V_4 = \{e''_{11}, e'_{12}, e'_{32}, e_{42}\}$ and $E_4 = \{e''_{11}e'_{12}, e''_{11}e'_{32}, e'_{32}e_{42}\}$. The process continues all the tracts are exhausted.

We compared topological properties between the networks constructed by the static and dynamic ε-neighbor methods. The networks constructed by the static ε-neighbor method had significantly more nodes (p-value < 0.05) at all ε-radii 7, 7.5, . . . 11.5, 12 and significantly fewer edges (p-value < 0.05) at ε-radii 10, 10.5, 11, 11.5, 12 than the dynamic method.

All the topological properties are statistically different between the statistic and dynamic methods (p-value < 0.05). Unlike the static method, we could not observe any significant difference in topological properties between the normal control subjects and the subjects with autism in the dynamic method. The networks constructed by the dynamic method have different topological organization as well as lacks the sensitivity to detect subtle network differences.

VII. Discussion

Structural brain networks consist of sets of nodes (brain regions) linked by edges (white matter tracts). Previous studies have used existing parcellations to identify the network nodes [2], [6], [7]. However, this method is problematic in that network structures are influenced by changes in the parcellation scale and thresholding in connectivity matrices. To overcome these problems, we proposed the ε-neighbor method.

We also examined how connectedness changes according to the network scale. Since some nodes remained disconnected from the largest connected component, connectedness decreased when the parcellation method was used and the parcellation scale becomes finer (Fig. 12). Due to the increase in number of disconnected nodes, topological properties such as clustering coefficient, average path length, and small-worldness do not meaningfully characterize network structures in the parcellation method [51].

In the proposed method, connectedness did not change with the network scale (ε-radius). In the ε-neighbor method, network connectedness remained at a high level even as the number of nodes increased. Thus, the topological properties of network can be characterized in a more meaningfully manner in the

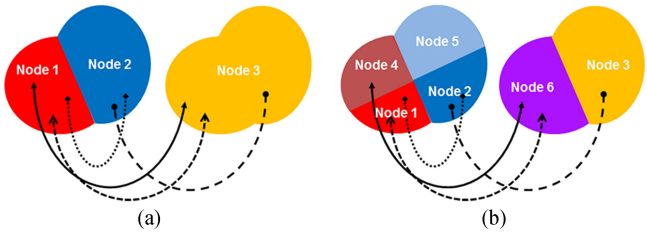

Fig. 12. Example of decreased connectedness in the parcellation method. (a) All nodes (parcellations) are intersected by tracts. (b) Node 5 is not intersected by any tract. Connectedness decreases in the parcellation method as the parcellation scale becomes finer.

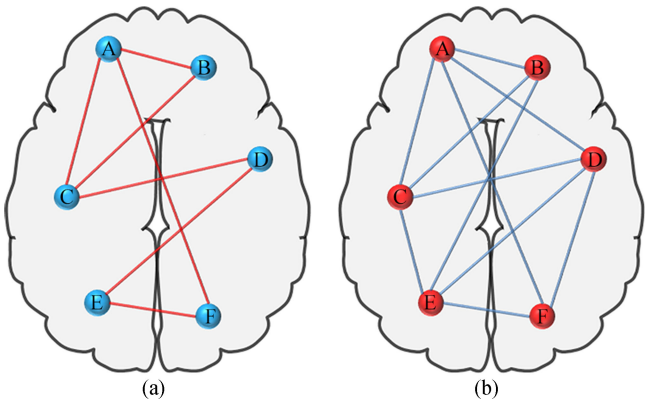

Fig. 13. (a) Typical connectivity in the normal controls. (b) Over-connectivity in autism. Subjects with autism have shorter path length, higher global efficiency, higher density, and higher node degree.

ε-neighbor method [51]. Our method is more realistically modeling the brain than the parcellation method.

Using fMRI and DTI, previous studies have tested the pervading hypothesis that brain connectivity in autism is abnormal [12], [17]. We observed significant differences between networks constructed from control subjects and subjects with autism with respect to path length, global efficiency, node degree, and density. More randomly connected networks tend to have shorter path lengths and higher global efficiency than more structured networks [52], which may reflect less organization in the former [9], [18].

From the results of shorter average path length, higher global efficiency, higher density, and higher degree in autism, we concluded that subjects with autism exhibited over-connected brain networks (Fig. 13). Since the presence of structural connections between two brain regions implies strong functional connections [53], over-connected structural brain network may be related with functional over-connectivity. The over-connectivity could cause the increase of synaptic excitation and decrease of synaptic inhibition. Imbalance of synaptic reaction could lead to functional deficits observed in autism [54].

We examined the structural characteristics of the brain networks in autism using the targeted node attack. We observed statistically significant differences in the size of the largest connected components. The size of the largest connected component is more steadily preserved in autism in the targeted node attacks. A more tolerant network for the targeted node attacks in autism implies that the network has more potential alternative paths and possible over-connectivity [27].

To identify regional abnormality caused by the structural over-connectivity in autism, we computed the regional efficiency. Subjects with autism had increased regional efficiency in the right superior temporal gyrus and the left middle temporal gyrus. These affected regions are consistent with those reported in previous studies based on fMRI, electroencephalogram (EEG), and DTI [55]–[59]. Temporal gyrus is critical pathways involved in language and social cognition. Abnormalities of this region may be causative of the neurobehavioral features observed in autism [58]. Superior temporal gyrus is connected to regions of association and limbic system [60] and may be crucial in face and gaze processing [61] and is related to emotional responses which also related to social cognition including visual, auditory and olfactory [62].

Acknowledgment

The authors would like to thank Kim M. Dalton and Nagesh Adluru of Waisman Center at the University of Wisconsin-Madison, and S.-G. Kim of Max Planck Institute for valuable discussions and image preprocessing supports.

References

[1] O. Sporns *et al.*, "Organization, development and function of complex brain networks," *Trends Cogn. Sci.*, vol. 8, no. 9, pp. 418–425, 2004.
[2] G. Gong *et al.*, "Mapping anatomical connectivity patterns of human cerebral cortex using in vivo diffusion tensor imaging tractography," *Cerebral Cortex*, vol. 19, no. 13, pp. 524–536, 2009.
[3] O. Sporns *et al.*, "The human connectome: A structural description of the human brain," *PLoS Comput. Biol.*, vol. 1, no. 4, 2005, Art. no. e42.
[4] M. Rubinov and O. Sporns, "Complex network measures of brain connectivity: Uses and interpretations," *Neuroimage*, vol. 52, no. 3, pp. 1059–1069, 2010.
[5] M. A. Just *et al.*, "Functional and anatomical cortical underconnectivity in autism: Evidence from an fMRI study of an executive function task and corpus callosum morphometry," *Cerebral Cortex*, vol. 17, no. 4, pp. 951–961, 2007.
[6] A. Zalesky *et al.*, "Whole-brain anatomical networks: Does the choice of nodes matter?," *Neuroimage*, vol. 50, no. 3, pp. 970–983, 2010.
[7] Q. Cao *et al.*, "Probabilistic diffusion tractography and graph theory analysis reveal abnormal white matter structural connectivity networks in drug-naive boys with attention deficit/hyperactivity disorder," *J. Neurosci.*, vol. 33, no. 26, pp. 10676–10687, 2013.
[8] M. K. Chung *et al.*, "Scalable brain network construction on white matter fibers," *Proc. SPIE*, vol. 7962, 2011, Art. no. 79624G.
[9] E. L. Dennis *et al.*, "Altered structural brain connectivity in healthy carriers of the autism risk gene, CNTNAP2," *Brain Connectivity*, vol. 1, no. 6, pp. 447–459, 2011.
[10] American Psychiatric Association, "Diagnostic statistical manual of mental disorders," Amer. Psychiatric Assoc., Washington, DC, USA, 1994.
[11] R. K. Kana *et al.*, "Brain connectivity in autism," *Frontiers Human Neurosci.*, vol. 8, 2014, Art. no. 349.
[12] M. K. Belmonte *et al.*, "Autism and abnormal development of brain connectivity," *J. Neurosci.*, vol. 24, no. 42, pp. 9228–9231, 2004.
[13] V. L. Cherkassky *et al.*, "Functional connectivity in a baseline resting-state network in autism," *Neuroreport*, vol. 17, no. 16, pp. 1687–1690, 2006.
[14] N. M. Kleinhans *et al.*, "Abnormal function connectivity in autism spectrum disorders during face processing," *Brain*, vol. 131, pp. 1000–1012, 2008.
[15] R. A. Müller *et al.*, "Underconnected, but how? A survey of functional connectivity MRI studies in autism spectrum disorders," *Cerebral Cortex*, vol. 21, no. 10, pp. 2233–2243, 2011.
[16] N. Adluru *et al.*, "Characterizing brain connectivity using ε-radial nodes: Application to autism classification," presented at the MICCAI Workshop Comput. Diffus. MRI, Beijing, China, 2010.

[17] M. K. Chung *et al.*, "Characterization of structural connectivity in autism using graph networks with DTI," presented at 16th Annu. Meeting Org. Human Brain Mapping, Barcelona, Spain, Jun. 6-10, 2010.

[18] J. D. Rudie *et al.*, "Altered functional and structural brain network organization in autism," *Neuroimage-Clin.*, vol. 2, no. 1, pp. 79–94, 2013.

[19] N. Tzourio-Mazoyer *et al.*, "Automated anatomical labeling of activations in SPM using a macroscopic anatomical parcellation of the MNI MRI single-subject brain," *Neuroimage*, vol. 15, no. 1, pp. 273–289, 2002.

[20] P. Hagmann *et al.*, "Mapping the structural core of human cerebral cortex," *PLoS Biol.*, vol. 6, no. 7, 2008, Art. no. e159.

[21] J. Leskovec and E. Horvitz, "Planetary-scale views on an instant-messaging network," in *Proc. 17th Int. World Wide Web Conf.*, 2008, pp. 915–924.

[22] D. J. Watts and S. H. Strogatz, "Collective dynamics of 'small-world' networks," *Nature*, vol. 393, pp. 440–442, 1998.

[23] P. Hagmann *et al.*, "Mapping human whole-brain structural networks with diffusion MRI," *PLoS One*, vol. 2, no. 7, 2007, Art. no. e597.

[24] V. Latora and M. Marchiori, "Efficient behavior of small-world networks," *Phys. Rev. Lett.*, vol. 87, no. 19, 2001, Art. no. 198701.

[25] A. J. Lawrence *et al.*, "Structural network efficiency is associated with cognitive impairment in small-vessel disease," *Neurology*, vol. 83, no. 4, pp. 304–311, 2014.

[26] E. T. Bullmore and D. S. Bassett, "Brain graphs: Graphical models of the human brain connectome," *Annu. Rev. Clin. Psycho.*, vol. 7, pp. 113–140, 2011.

[27] B. C. Bernhardt *et al.*, "Graph-theoretical analysis reveals disrupted small-world organization of cortical thickness correlation networks in temporal lobe epilepsy," *Cerebral Cortex*, vol. 21, no. 9, pp. 2147–2157, 2011.

[28] P. Holme *et al.*, "Attack vulnerability of complex networks," *Phys. Rev. E*, vol. 65, no. 5, 2002, Art. no. 056109.

[29] P. Holme *et al.*, "Attack vulnerability of complex networks," *Phys. Rev. E*, vol. 65, no. 5, 2002, Art. no. 056109.

[30] V. M. Eguíluz *et al.*, "Scale-free brain functional networks," *Phys. Rev. Lett.*, vol. 94, no. 1, 2005, Art. no. 018102.

[31] M. Kaiser, "A tutorial in connectome analysis: Topological and spatial features of brain networks," *Neuroimage*, vol. 57, no. 3, pp. 892–907, 2011.

[32] T. F. Coleman and J. J. Moré, "Estimation of sparse jacobian matrices and graph coloring problems," *SIAM J. Numer. Anal.*, vol. 20, no. 1, pp. 187–209, 1983.

[33] A. Pothen and C. J. Fan, "Computing the block triangular form of a sparse matrix," *ACM Trans. Math. Softw.*, vol. 16, no. 4, pp. 303–324, 1990.

[34] T. H. Hsieh *et al.*, "Diagnosis of schizophrenia patients based on brain network complexity analysis of resting-state fMRI," in *Proc. 15th Int. Conf. Biomed. Eng.*, 2014, pp. 203–206.

[35] A. Fornito *et al.*, "Network scaling effects in graph analytic studies of human resting-state fMRI data," *Frontiers Syst. Neurosci.*, vol. 4, 2010, Art. no. 22.

[36] J. M. Anthonisse, "The rush in a directed graph," Stichting Mathematisch Centrum, Amsterdam, The Netherlands, *Tech. Rep. BN 9/71*, 1971.

[37] L. C. Freeman, "A set of measures of centrality based on betweenness," *Sociometry*, vol. 40, no. 1, pp. 35–41, 1977.

[38] T. E. Nichols and A. P. Holmes, "Nonparametric permutation tests for functional neuroimaging: A primer with examples," *Human Brain Mapping*, vol. 15, no. 1, pp. 1–25, 2001.

[39] D. Fein, *The Neuropsychology of Autism*. New York, NY, USA: Oxford Univ. Press, 2011, ch. 3, pp. 51–52.

[40] A. Yandiki *et al.*, "Spurious group differences due to head motion in a diffusion MRI study," *Neuroimage*, vol. 88, pp. 79–90, 2014.

[41] R. P. Woods *et al.*, "Automated image registration: I. General methods and intrasubject, intramodality validation," *J. Comput. Assisted Tomography*, vol. 22, no. 1, pp. 139–152, 1998.

[42] P. Jezzard and R. S. Balaban, "Correction for geometric distortion in echo planar images from B0 field variations," *Magn. Reson. Med.*, vol. 34, no. 1, pp. 65–73, 1995.

[43] D. C. Alexander and G. J. Barker, "Optimal imaging parameters for fiber-orientation estimation in diffusion MRI," *Neuroimage*, vol. 27, no. 2, pp. 357–367, 2005.

[44] H. Zhang *et al.*, "High-dimensional spatial normalization of diffusion tensor images improves the detection of white matter differences: An example study using amyotrophic lateral sclerosis," *IEEE. Trans. Med. Imag.*, vol. 26, no. 11, pp. 1585–1597, Nov. 2007.

[45] P. A. Cook *et al.*, "Camino: Open-source diffusion-MRI reconstruction and processing," in *Proc. 14th Sci. Meeting Int. Soc. Magn. Reson. Med.*, 2006, p. 2759.

[46] M. Lazar *et al.*, "White matter tractography using diffusion tensor deflection," *Human Brain Mapping*, vol. 18, no. 4, pp. 306–321, 2003.

[47] A. Gruslys *et al.*, "3000 non-rigid medical image registrations overnight on a single PC," in *Proc. IEEE Nucl. Sci. Symp. Med. Imag. Conf.*, 2011, pp. 3073–3080.

[48] L. A. N. Amaral *et al.*, "Classes of small-world networks," *Proc. Nat. Acad. Sci.*, vol. 97, pp. 11149–11152, 2000.

[49] S. R. Kesler *et al.*, "Brain network alterations and vulnerability to simulated neurodegeneration in breast cancer," *Neurobiol. Aging*, vol. 36, no. 8, pp. 2429–2442, 2015.

[50] E. D. Fagerholm *et al.*, "Disconnection of network hubs and cognitive impairment after traumatic brain injury," *Brain*, vol. 138, no. 6, pp. 1696–1709, 2015.

[51] J. Qin *et al.*, "Altered anatomical patterns of depression in relation to antidepressant treatment: Evidence from a pattern recognition analysis on the topological organization of brain networks," *J. Affective Disorders*, vol. 180, pp. 129–137, 2015.

[52] K. Supekar *et al.*, "Network analysis of intrinsic functional brain connectivity in Alzheimer's disease," *PLoS Comput. Biol.*, vol. 4, no. 6, 2008, Art. no. e1000100.

[53] E. Bullmore and O. Sporns, "Complex brain networks: Graph theoretical analysis of structural and functional systems," *Nat. Rev. Neurosci.*, vol. 10, no. 3, pp. 186–198, 2009.

[54] Z. Wang *et al.*, "The relationship of anatomical and functional connectivity to resting-state connectivity in primate somatosensory cortex," *Neuron*, vol. 78, no. 6, pp. 1116–1126, 2013.

[55] K. Supekar *et al.*, "Brain hyperconnectivity in children with autism and its links to social deficits," *Cell Rep.*, vol. 5, no. 3, pp. 738–747, 2013.

[56] N. Barnea-Goraly *et al.*, "White matter structure in autism: preliminary evidence from diffusion tensor imaging," *Biol. Psychiatry*, vol. 55, no. 3, pp. 323–326, 2004.

[57] G. Dawson *et al.*, "Subgroups of autistic children based on social behavior display distinct patterns of brain activity," *J. Abnormal Child Psychol.*, vol. 23, no. 5, pp. 569–583, 1995.

[58] P. G. Enticott *et al.*, "Electrophysiological signs of supplementary-motor-area deficits in high-functioning autism but not Asperger syndrome: An examination of internally cued movement-related potentials," *Developmental Med. Child Neurol.*, vol. 51, no. 10, pp. 787–791, 2009.

[59] J. E. Lee *et al.*, "Diffusion tensor imaging of white matter in the superior temporal gyrus and temporal stem in autism," *Neurosci. Lett.*, vol. 424, no. 2, pp. 127–132, 2007.

[60] J. G. Levitt *et al.*, "Cortical sulcal maps in autism," *Cerebral Cortex*, vol. 13, no. 7, pp. 728–735, 2003.

[61] R. J. Jou *et al.*, "Enlarged right superior temporal gyrus in children and adolescents with autism," *Brain Res.*, vol. 1360, pp. 205–212, 2010.

[62] A. Puce *et al.*, "Temporal cortex activation in humans viewing eye and mouth movements," *J. Neurosci.*, vol. 18, no. 6, pp. 2188–2199, 1998.